Draft version January 30, 2002
Preprint typeset using LaTeX style emulateapj v. 20/04/00

MEASUREMENTS OF SOLAR IRRADIANCE AND EFFECTIVE TEMPERATURE AS A PROBE OF SOLAR INTERIOR MAGNETIC FIELDS

L. H. Li[1,2] and S. Sofia
Department of Astronomy, Yale University, P.O. Box 208101, New Haven, CT 06520-8101
Draft version January 30, 2002

ABSTRACT

We argue that a variety of solar data suggest that the activity-cycle timescale variability of the total irradiance, is produced by structural adjustments of the solar interior. Assuming these adjustments are induced by variations of internal magnetic fields, we use measurements of the total irradiance and effective temperature over the period from 1978 to 1992, to infer the magnitude and location of the magnetic field. Using an updated stellar evolution model, which includes magnetic fields, we find that the observations can be explained by fields whose peak values range from 120k to 2.3k gauss, located in the convection zone between $0.959R_\odot$ and $0.997R_\odot$, respectively. The corresponding maximal radius changes, are 17 km when the magnetic field is located at $0.959R_\odot$ and 3 km when it is located at $0.997R_\odot$. At these depths, the W parameter (defined by $\Delta \ln R/\Delta \ln L$, where R and L are the radius and luminosity) ranges from 0.02 to 0.006. All these predictions are consistent with helioseismology and recent measurements carried out by the MDI experiment on SOHO.

Subject headings: Sun: interior — Sun: magnetic fields

1. INTRODUCTION

Direct satellite measurements of total solar irradiance (Willson & Hudson 1991; Fröhlich & Lean 1998), show that it varies almost in phase with the solar activity cycle, and that its relative variation in amplitude is about 0.1%. Although the most common explanation of this change, involves the effect of magnetic regions and network (superposed to an otherwise constant solar photosphere), an alternative explanation is that the cyclic variation is primarily due to structural changes of the solar interior. Two arguments support this second possibility. Firstly, direct measurements of the spectrum of p-mode oscillations, show variations (Libbrecht & Woodard 1990) that can be best explained in terms of structural changes (i.e. changes in pressure, density, radius, etc) (Lydon et al 1996; Antia et al 2000; Balmforth et al 1996). Secondly, measurements of the "effective temperature" by Gray and Livingston (1997b), also vary nearly in phase with the solar cycle. This variation is obtained by monitoring the neutral carbon λ5380 line in the solar flux spectrum. They present several arguments supporting their contention that what they measure is the gas temperature in the deep photosphere, free from the influence of sunspots, faculae and small scale magnetic flux tubes. Their main argument rests on their simultaneous monitoring of C I λ5380, Fe I λ5379 and Ti II λ5381. They use the ratios of spectral line depths, C I λ5380 to Fe I λ5379 and to Ti II λ5381, as temperature indicators. Since these three lines have different excitation potentials (1.57 eV for Ti II λ5381, 3.69 eV for Fe I λ5379, and 7.68 eV for C I λ5380), the consistency of the results for the two line depth ratios, shows that the temperature indicators are free from the influence of variations of faculae and small scale magnetic flux tubes, which would be expected to affect each line in a different way. See Gray & Livinston (1997a,b) for the entire discussion. In order for the gas temperature to change, the energy flow from the interior must also change. Structural adjustment will be able to accomplish this. Since the relative radius variation $\Delta \ln R$ is very small (Emilio et al 2000),

$$\Delta \ln L \approx 4\Delta \ln T, \qquad (1)$$

where L and T are luminosity and temperature, respectively. The temperature change measured by Gray and Livingston (1997) is 1.5 ± 0.2 K in one cycle, which corresponds to $\Delta \ln T \sim 0.025\%$ and $\Delta \ln L \sim 0.1\%$. This is approximately the entire cyclic variation of the total irradiance.

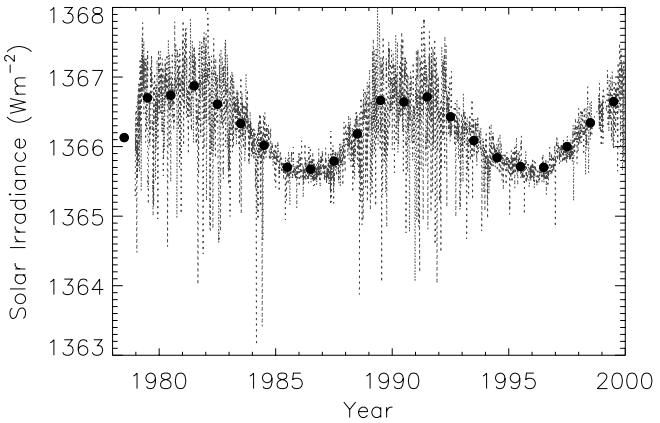

FIG. 1.— A composite solar irradiance record from the end of 1978 to the present (Fröhlich & Lean 1998) and the yearly mean of solar irradiance.

The most obvious way the solar structure may change, is in response to variations of the internal magnetic field during the dynamo build-up and decay. In order to compute this effect, we introduce magnetic variables as new stellar structure variables (Lydon & Sofia 1995), in addi-

[1]also at Purple Mountain Observatory, Chinese Academy of Sciences
[2]also at National Astronomical Observatories, Chinese Academy of Sciences

tion to the conventional ones (Guenther et al 1992). Since magnetic field is not a scalar, we have to use at least two variables to describe it: the magnetic energy density χ (Lydon & Sofia 1995), and the ratio of the magnetic pressure to the magnetic energy, $\gamma-1$ (Endal et al 1985). This method was developed by Lydon and Sofia in 1995, in which γ was treated as a parameter, and it was subsequently applied by Lydon, Guenther and Sofia (1996), to explain the observed variation of solar p-mode oscillations with the solar cycle (Libbrecht & Woodard 1990). Here we want to update this method by: (i) treating both χ and γ as new structure variables, as done for χ in Lydon and Sofia (1995), (ii) taking into account the influence of magnetic fields on radiative opacities, (iii) taking into account all time-dependent contributions to the equations of stellar structure (since we want to treat short time scales), (iv) modifying the radiative loss assumption of a convective element (as discussed in section 3), (v) updating the code by using the new version of Yale Stellar Evolution Code (YREC7) and (vi) removing the perfect gas approximation, which was assumed when calculating some first- and second-order derivatives associated with magnetic fields in Lydon and Sofia (1995). Because luminosity, radius and temperature variations are sensitive to the location, intensity, orientation, and distribution of the perturbation magnetic field $B = (8\pi\chi\rho)^{1/2}$ (ρ is the gas density), we can use the measured yearly-averaged irradiance, temperature and radius variations, to determine the solar interior magnetic field as a function of mass and time.

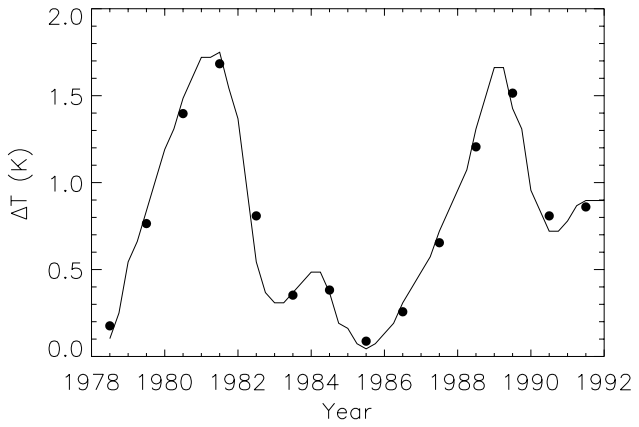

FIG. 2.— The measured solar photospheric temperature variations from 1978 to 1992 (Gray & Livingston 1997b) and the yearly mean.

2. SOLAR IRRADIANCE AND EFFECTIVE TEMPERATURE RECORDS

Space-based solar irradiance measurements have been reviewed by Fröhlich and Lean (1998), and a composite solar irradiance record for the period from 1978 to the present can be downloaded from the website http://www.ngdc.noaa.gov/. In our magnetic perturbation model calculations, we use one year as the timestep, since variations on the shorter time scales may be attributed to the effect of magnetic regions and network. We compare the results with the yearly means of total solar irradiance, as shown in Figure 1. The standard variances range from 0.1 Wm^{-2} to 0.5 Wm^{-2}.

The spectroscopic temperature variations of the sun, measured by Gray and Livingston (1997) over the period from 1978 to 1992, are shown in Figure 2 (reproduced from their Figure 9). The points are the yearly means, the zero point being chosen arbitrarily.

3. METHOD

3.1. *Definition of variables*

Standard solar models (SSM) use pressure, temperature, radius and luminosity as the structure variables, and mass M_r interior to a radius r, as the independent variable. In order to self-consistently take into account magnetic effects, Lydon and Sofia (1995) introduced two new magnetic structure variables to model the sun: the magnetic energy per unit mass χ, and the effective ratio of specific heats for the magnetic perturbation, γ. The former describes the magnetic perturbation strength, and the latter describes the tensor feature of the magnetic pressure. In general, the determination of χ and γ requires a comprehensive understanding of turbulent dynamics in the solar convective zone (Brummell et al 1995), an undertaking that is impractical at present. Therefore we take χ and γ as free parameters (functions) that need to be determined at this stage, instead of using dynamo equations to determine them.

Our aim is to use the measured solar irradiance and effective temperature variations given in Figures 1 and 2 to determine $\chi(M_D,t)$ and $\gamma(M_D,t)$, where M_D and t are mass depth and time, respectively. Using $\chi(M_D,t)$, we can obtain the solar interior magnetic field $B(M_D,t) = (8\pi\chi\rho)^{1/2}$. Since these observations are not enough to determine the two new variables uniquely, we assume they have a gaussian-like shape, and also utilize helioseismic ((Antia et al 2000)) and radius ((Emilio et al 2000)) observations, as additional constraints. The mass depth M_D is defined as

$$M_D = \log_{10}(1 - M_r/M_\odot). \quad (2)$$

This replaces the mass variable M_r when we want to describe the location, orientation and form of all magnetic perturbations.

For our purpose we can use the toroidal (B_t) and poloidal (B_p) components to express a magnetic field vector $\vec{B} = (B_t, B_p)$. The magnetic energy density variable χ can be written as,

$$\chi = (B^2/8\pi)/\rho, \quad (3)$$

where $B = (B_t^2 + B_p^2)^{1/2}$ is the magnitude of the magnetic field vector. The magnetic field direction variable γ can be written as,

$$\gamma = (2B_t^2 + B_p^2)/B^2. \quad (4)$$

The magnetic pressure P_χ can be defined in terms of the new magnetic variables as

$$P_\chi = (\gamma - 1)\chi\rho. \quad (5)$$

The value of γ depends on the field geometry. Parallel to the field lines, P_χ is zero, so $\gamma = 1$, whereas perpendicular to the field lines, P_χ is a maximum, so $\gamma = 2$.

3.2. *Consequences on the equations of stellar structure*

The continuity equation remains the same. The hydrostatic equation is replaced by the equation of motion, which including the Lorentz force, is

$$\rho\frac{\partial^2\vec{r}}{\partial t^2} = -\nabla P - \frac{GM_r}{r^2}\rho\hat{r} + \frac{1}{4\pi}(\nabla\times\vec{B})\times\vec{B},$$

where G is the gravitational constant. The radial component is

$$\rho\frac{\partial^2 r}{\partial t^2} = -\frac{\partial P}{\partial r} - \frac{GM_r}{r^2}\rho - \frac{\partial P_\chi}{\partial r}.$$

The magnetic field has both a magnetic tension and a magnetic pressure. This can be seen by writing the Lorentz force $(1/4\pi)(\nabla \times \vec{B}) \times \vec{B}$, as the sum of the magnetic tension $(\vec{B}\cdot\nabla)\vec{B}/4\pi$ and the magnetic pressure $-\nabla(B^2/8\pi)$. The former is anisotropic, and the latter is isotropic. Both contribute to the last term of the radial motion equation, and are incorporated into P_χ. For example, for a purely radial magnetic field, the magnetic tension force, $(1/4\pi)B_r\partial B_r/\partial r = (1/8\pi)\partial B_r^2/\partial r = (1/8\pi)\partial B^2/\partial r$, which cancels the magnetic pressure force. As a result, $P_\chi = 0$ in this case.

Defining

$$P_T = P + P_\chi$$

as the total pressure, the equation of radial motion becomes

$$\frac{\partial P_T}{\partial M_r} = -\frac{GM_r}{4\pi r^4} - \frac{1}{4\pi r^2}\frac{\partial^2 r}{\partial t^2}, \tag{6}$$

where the last term represents the inertial force. Since

$$\rho = \rho(P_T, T, \chi, \gamma),$$

the equation of state becomes

$$\frac{d\rho}{\rho} = \alpha\frac{dP_T}{P_T} - \delta\frac{dT}{T} - \nu\frac{d\chi}{\chi} - \nu'\frac{d\gamma}{\gamma},$$

where

$$\alpha = \frac{\partial \ln\rho}{\partial \ln P_T} \text{ at constant T, } \chi, \gamma$$

$$\delta = -\frac{\partial \ln\rho}{\partial \ln T} \text{ at constant } P_T, \chi, \gamma$$

$$\nu = -\frac{\partial \ln\rho}{\partial \ln\chi} \text{ at constant } P_T, \text{ T}, \gamma$$

$$\nu' = -\frac{\partial \ln\rho}{\partial \ln\gamma} \text{ at constant } P_T, \text{ T}, \chi$$

Since we use the one-dimensional stellar evolution model, we can not model the transverse component of the equation of motion. In order to handle this transverse component, we need at least a two-dimensional stellar evolution model. Since such a model is not available yet, we only consider the radial motion equation in this paper.

The energy conservation equation becomes

$$\frac{\partial L}{\partial M_r} = \epsilon - T\frac{dS_T}{dt} - \frac{1}{\rho}\frac{\partial u}{\partial t}. \tag{7}$$

Here

$$\begin{aligned} TdS_T &= dQ_T = dU + PdV + d\chi \\ &= dU_T + P_T dV - (\gamma-1)(\chi/V)dV \\ &= c_{\rm p}dT - \frac{\delta}{\rho}dP_T + \left(1 + \frac{P_T\delta\nu}{\rho\alpha\chi}\right)d\chi + \frac{P_T\delta\nu'}{\rho\alpha\gamma}d\gamma \end{aligned} \tag{8}$$

is the first law of thermodynamics including magnetic fields. The total internal energy $U_T = U + \chi$ and the total entropy $S_T = S + \chi/T$. $c_{\rm p}$ is the specific heat at constant pressure. If γ is constant, then $d\gamma = 0$, and equation (8) reduces to equation (75) in Lydon & Sofia (1995). The symbol $u = aT^4$, is the radiation energy density, where a is the radiation constant. $\partial u/\partial t$ appears in the full energy conservation equation,

$$\frac{\partial u}{\partial t} + \nabla\cdot\vec{F} = \rho(\epsilon - T\frac{dS_T}{dt}).$$

$\vec{F} = u\vec{v}$ is the radiation energy flux vector, and $\vec{v}$ is the photon diffusion velocity.

The equation of transport of energy by radiation,

$$\frac{\partial T}{\partial M_r} = -\frac{3}{64\pi^2 ac}\frac{\kappa l}{r^4 T^3}, \tag{9}$$

does not change in form, but the magnetic field affects the opacity coefficient κ. Here c is the speed of light. See appendix A for an estimate of this effect.

The equation of energy transport by convection,

$$\frac{\partial T}{\partial M_r} = -\frac{T}{P}\frac{GM_r}{4\pi r^4}\nabla, \tag{10}$$

does not change form either, but the convection temperature gradient, ∇, with a magnetic field, is different from that without it. Lydon and Sofia (1995) have demonstrated how to account for magnetic effects in the mixing length theory, and hence obtain ∇, provided γ is constant. Their method can also be used to derive ∇ when γ is variable, as we are about to do in this paper. See appendix B for the concrete expression for ∇ in our case.

3.3. *Numerical implementation*

The stellar evolution code solves the stellar structure equations (such as Eqs. [6], [7] and [9] or [10], and the continuity equation, $\partial r/\partial M_r = 1/4\pi r^2\rho$), with suitable initial and boundary conditions. In the model, M_r and t are the independent variables, and the conventional structure variables are P_T, T, r and L, while the magnetic variables are χ and γ.

To follow the yearly variations of solar global parameters with a stellar evolution code, requires a timestep no larger than one year. Such a small timestep requires a very precise code. For example, because $L_\odot$ has increased by about 30% during the lifetime of the sun, the relative mean rate of change is about 10^{-10} per year. To achieve such a high precision is a challenge. Fortunately, Yale stellar evolution code (YREC) meets this need, as shown before, (Lydon & Sofia 1995). We follow Lydon and Sofia (1995) by modifying YREC7, a new version released in May 1999, in order to accommodate the magnetic effects described above. The reason why YREC permits a small timestep and achieves such a high numerical precision, is because it uses analytical formulae (Prather 1976), rather than numerical methods, to solve the linearized stellar structure equations.

In order to accommodate the various magnetic effects described above, we must first write a routine to specify χ and γ. We assume $\chi = \chi_m(t)F(M_D)$. The maximum magnetic energy density $\chi_m(t)$, is to be determined from solar activity indices. The yearly-averaged sunspot number, R_Z, is the most widely used solar activity index. From numerical experiments, we find that the results are sensitive to the function form of B_m on R_z. If the maximum magnetic field in the solar interior, B_m, is related to R_Z via

$$B_m = B_0\{190 + [1 + \log_{10}(1 + R_Z)]^5\}, \tag{11}$$

then by adjusting B_0, we can nearly match the measured cyclic variations of irradiance and effective temperature.

The reason why such a functional form of B_m is chosen is that $B \sim 20$ kG, at a depth of $M_D = -4.25$ ($r = 0.96 R_\odot$) in 1996. This result is inferred from helioseismology (Antia et al 2000) when R_Z was at a minimum. Using this prescription for B_m, the value of B_m is about twice as large at the maximum of solar cycle, as it is at the minimum.

$F(M_D)$ specifies the distribution of χ, and is to be determined by fitting the measured irradiance and effective temperature variations. $F(M_D)$ has infinite degrees of freedom and thus cannot be determined uniquely by observational results, which have finite degrees of freedom. However, we can remove this degeneracy by assuming a field shape of the form,

$$F(M_D; M_{\rm Dc}, \sigma) = \exp[-\tfrac{1}{2}(M_D - M_{\rm Dc})^2/\sigma^2], \qquad (12)$$

where $M_{\rm Dc}$ specifies the location and σ specifies its width. This gaussian profile allows us to pinpoint the location of the required magnetic field, by using observations of cyclic variations of irradiance and effective temperature.

We either fix γ, or use

$$\gamma(M_D) = 1 + (B/B_m)^{1/5}(R_Z/200), \qquad (13)$$

to express the spatial and temporal variations of the direction of magnetic fields. This implies that the more intense the magnetic field, the larger its toroidal component. The profile of γ is arbitrary, but its value must lie between 1 and 2. Although the detailed results are sensitive to the functional form of γ, the qualitative features are same. We find that the magnetic effects are maximized when $\gamma = 2$, so we set $\gamma = 2$ in subsequent computations. The main effect of a smaller γ, is to increase the magnetic field required to reproduce the observed variation of the sun.

As the magnetic fields that cause the solar activity cycle are believed to exist outside of the solar core (where the thermonuclear reactions occur), we do not consider the influence of magnetic fields on the energy generation rate.

Magnetic fields affect the equation of state in the following way. If β, the ratio of the gas pressure to the total pressure when magnetic fields are present, is defined as

$$\beta = 1 - \frac{\frac{1}{3}aT^4}{P_T} - \frac{(\gamma-1)\chi\rho}{P_T}, \qquad (14)$$

(a is the radiation constant), then the density of a gas can be determined from

$$\beta P_T = \mathcal{R}\rho T(1+E)/\mu_a. \qquad (15)$$

$\mathcal{R}$ is the gas constant, E is the number of free electrons per nucleus (determined by solving the Saha equation) and μ_a is the mean atomic weight per atom (Prather 1976). Note, E also depends on β. In the stardard case, since $\chi = 0$, β does not depend on ρ. But in the nonstandard case discussed in this paper, β depends on ρ. Consequently, not only ρ, but also its first derivatives α, δ, ν, and ν', and its second derivatives with respect to T and P_T, all need to be calculated by iteration (which is tedious). In the original implementation of this method by Lydon and Sofia (1995). The second derivatives were approximated by assuming a perfect gas, which needs no iteration. In this code upgrade, we modify the equation of state routine so that we can accurately calculate all these thermodynamic variables by iteration. Although this improves the numerical precision, it does not make any qualitative difference. ∇_χ and ∇_γ (defined in Appendix B) are also calculated by numerical derivatives, as are those time derivatives which appear in the equations of stellar structure.

The qualitative difference comes from f' (see Appendix B), which represents the influence of magnetic field on radiative loss of a convection element. The convection temperature gradient is now given by

$$\nabla = \nabla_{\rm ad} + (y'/V'\gamma_0^2 C)(1 + y'/V') - A_m, \qquad (16)$$

where

$$A_m = f'[(\nu/\alpha)\nabla_\chi + (\nu'/\alpha)\nabla_\lambda]\nabla_{\rm ad}. \qquad (17)$$

All symbols used here are defined in Appendix B. When $f' = 1$ and γ is fixed, equation (17) reduces to

$$A_m = (\nu/\alpha)\nabla_\chi\nabla_{\rm ad}. \qquad (18)$$

However, under those assumptions, the calculated cyclic variation of effective temperature is in antiphase with the solar activity, contrary to the observations (Gray & Livingston 1997b). In order to get a proper fit to the observations, it is necessary to assume $f' = 3$, a value that will be used in all our subsequent calculations.

We use Eq. (A2) to compute the global magnetic effect on the radiative opacity, and find that this has little influence on the effective temperature. On the other hand, the need of $f' = 3$ implies that the energy loss of a convective element due to turbulence associated with the local magnetic field, is much more efficient than the radiative loss enhancement of the convective element due to the global magnetic field.

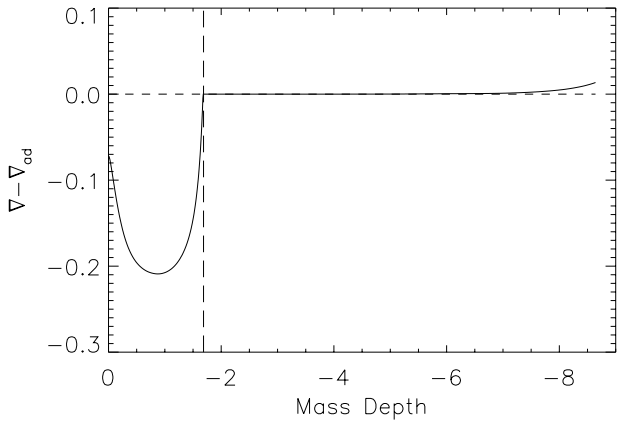

FIG. 3.— The difference between the temperature gradient and the adiabatic gradient as a function of the mass depth in the solar interior. The dashed line marks the location of lower boundary surface of the convection zone.

We do not redistribute the mass grid points, nor do we predict stellar structure variables for the next time step, when the timestep is smaller than a solar cycle period, since these operations will generate an error much larger than 10^{-10} per year for luminosity. All convergence criteria for iteration are tightened by requiring the relative error to be no larger than 6×10^{-16} or so. In this modified code, the matching point is at $M_D \approx -8.6$.

The conventional model parameters are, the mixing length parameter (the ratio of the mixing length to the pressure scale height, usually denoted as α parameter), the initial hellium mass abundance (Y_0), and the initial heavy element mass abundance (Z). The magnetic parameters introduced in this paper are the peak mass depth $M_{\rm Dc}$ of the magnetic energy density χ, the width of χ (i.e.,σ),

the magnetic strength parameter B_0, and the turbulent loss parameter of energy of a convective element f'. It is well known that the conventional parameters can be determined by present observations of solar radius and luminosity. Through numerical experiments (i.e., model calculations), we find that the magnetic parameters ($M_{\rm Dc}$, σ, B_0 and f'), can be determined by the observed cyclic variation of solar radius, luminosity and effective temperature. We fix $f' = 3$ in all subsequent runs, as required by the observed variation of effective temperature. $\gamma = 2$ is fixed to maximize the magnetic effects. In order to probe the observation-required location, strength and profile of the solar interior magnetic field, we change $M_{\rm Dc}$, σ and B_0 from run to run.

4. CONSTRAINTS ON THE SOLAR INTERIOR MAGNETIC FIELD

4.1. *The overshoot layer*

At present, it is generally believed that the magnetic field is stored only in the subadiabatically stratified overshoot layer in the form of flux tubes, which may break loose due to kink instabilities, when a threshold of 10^5 gauss is exceeded (Caligar et al 1995; Caligar et al 1998). Figure 3 depicts $\nabla - \nabla_{\rm ad}$ vs M_D, in which the subadiabatically stratified overshoot layer approximately corresponds to the mass depth range: $-1.68 \leq M_D < -1.2$. $M_{\rm Dc} = -1.68$ marks the base of the convection zone of our model sun. Therefore, the maximum yearly-averaged field strength B_m in the overshoot layer during the solar cycle should be smaller than the threshold. The field with $M_{\rm Dc} = -1.45$ and $\sigma < 0.2$, can be considered to be confined in the overshoot layer. However, even if the threshold value of B is used, the resultant irradiance and effective temperature variations are negligible.

Only when we abandon this threshold constraint (e.g., using a field larger than 2.6×10^6 gauss), can we get irradiance variations comparable to the observations, in magnitude and phase; however, even then, the effective temperature variation is much smaller and in antiphase with the solar cycle. Besides, the resulting relative radius variation is larger than 0.03%. Since the observations reveal that both irradiance and effective temperature variations are in phase with the solar cycle, and the relative radius variation should be much smaller than 0.01% (Emilio et al 2000), we conclude that the magnetic field that gives rise to the observed variations of irradiance and effective temperature (shown in Figures 1 and 2) cannot be completely confined in the overshoot layer.

4.2. *The convection zone*

The above arguments lead us to investigate the possibility that the magnetic field is located totally within the convection zone. We set $\sigma = 0.5$ in this region. In order to reproduce the observed cyclic variation of irradiance and effective temperature, B_0 will increase if σ decreases, and vice versa. We choose $M_{\rm Dc}$ from the interval (-8.6,-1.68], which covers the convection zone of our numerical solar model. For each selected value for $M_{\rm Dc}$, we change B_0 in order to reproduce the observed cyclic variations of solar irradiance and effective temperature by using our solar evolution code.

4.2.1. *The lower part*

We find that the lower part of the convection zone, $-1.68 \geq M_{\rm Dc} > -4.2$, is ruled out because it produces radius changes that are too large ($\Delta \ln R > 0.01\%$) and/or because it requires a too strong magnetic field ($B > 5 \times 10^4$ G).

4.2.2. *The intermediate part*

For the next region up, $-4.2 > M_{\rm Dc} > -7.8$, or $0.959 R_\odot < R < 0.997 R_\odot$, we find that our model can reproduce the observed cyclic variations of irradiance and effective temperature by using a possible equipartition magnetic field, $B_m < 5 \times \times 10^4$ G. In this case, the amplitude of the radius changes is from 17 to 3 km, and $W = \Delta \ln R / \Delta \ln L$ ranges from 0.02 to 0.006.

In order to pinpoint the location of the required magnetic fields in the allowed region of solar convection zone ($M_{\rm Dc} \in [-7.8, -4.2]$), we need more information. We obtain the allowed region by using the observational information for solar irradiance and effective temperature cyclic variations, and by assuming the corresponding solar radius variation $\Delta \ln R$ to be much smaller than 0.01%. If we have the direct observational information for $\Delta \ln R$ or the W parameter, we can pinpoint the location of solar interior magnetic fields. Since we do not have simultaneous observational information for the radius cyclic variation in the period ranging from 1978 to 1992, we must invoke some physical considerations.

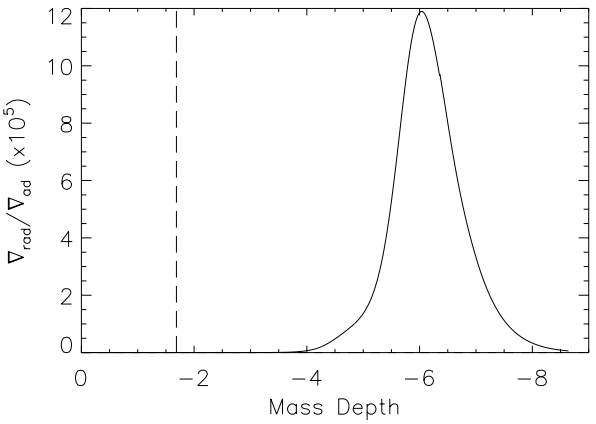

FIG. 4.— The ratio of radiative to adiabatic temperature gradients as a function of mass depth in the solar interior. The dashed line marks the location of lower boundary surface of the convection zone.

Figure 4 shows the ratio of radiative to adiabatic temperature gradients as a function of mass depth in the sun, from which we can see that the layer with M_D ranging from -4 to -8 is the most unstable convective region. In this layer superstrong plasma turbulence is inevitable, since the radiative gradient $\nabla_{\rm rad}$ is much larger than the adiabatic temperature gradient $\nabla_{\rm ad}$. Therefore, this may suggest a turbulence generation mechanism for solar magnetic fields. Strong plasma turbulence can generate strong small-scale magnetic fields, which form small magnetic cells with almost random orientation. The residual field of the previous cycle and differential rotation, tend to align and bundle these random magnetic "needles" to form flux tubes.

The solid curve in Figure 5 (choosing $M_{\rm Dc} = -6.5$, $\sigma = 0.5$, $B_0 = 7$ G) shows the corresponding magnetic field distribution in the solar interior in 1989, near solar maximum. Figure 6 compares the calculated (solid curve) and measured (dash-dotted curve) cyclic irradiance variation, while Figure 7 compares the calculated (solid curve) and measured (dash-dotted curve) cyclic effective temperature variation. The irradiance fit ($\chi^2 = 2$) is better than the effective temperature fit ($\chi^2 = 47$). The computed radius variation is 5×10^{-6}, and the W parameter is almost constant (about 4×10^{-3}). Figure 8 shows the calculated structure change generated by the field in 1989 (solid curve).

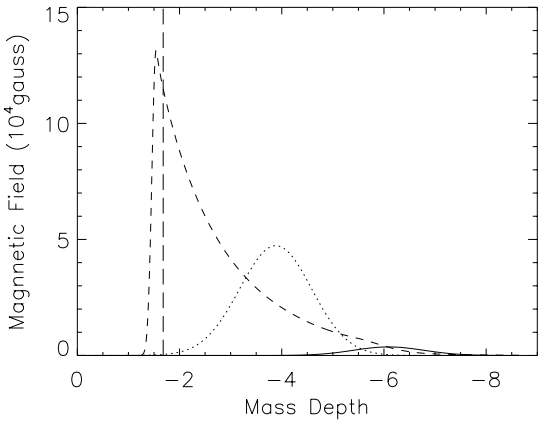

FIG. 5.— Three possible distributions of inferred magnetic field in the solar interior in 1989 according to the measured irradiance and photospheric temperature cyclic variations given in Figures 1 and 2. The vertical line indicates the base of the convection zone.

Although we can relate the magnetic field generation to the plasma turbulence in this region, the magnetic field maintenance here faces the old problem of magnetic buoyancy. How can we get around this problem? Observations and simulations suggest that the actual dynamics within solar convection zone is extremely intricate (Brummell et al 1995; Kim & Chan 1998; Nordlund 1999). The velocities and magnetic fields are complex, exhibiting large-scale structure and ordered behavior amidst rapidly varying and intense small-scale turbulence. In fact, the numerical simulations of the solar outer convection zone (Kim & Chan 1998; Nordlund 1999) indicate a major presence of downward moving plumes. These ordered downdrafts may gather small magnetic flux tubes, generated in the extremely unstable layer, to form larger flux tubes and carry them to the deeper layer. These downdrafts may also push down the magnetic flux tubes to balance the magnetic buoyancy to form a magnetized layer below the most unstable convective region.

One possibility is that the downdrafts gather and carry magnetic flux tubes, generated by turbulence, to depths in the convective envelope until some sort of equipartition is reached. In fact, Antia, Chitre, and Thompson (2000) have explored this possibility. They employ the observed splittings of solar oscillation frequencies to separate the effects of interior solar rotation, and to estimate the contribution from a large-scale magnetic field. After subtracting out the estimated contribution from rotation, there is some residual signal in the even splitting coefficients. This may be explained by a magnetic field of approximately 20 kG strength located at a depth of $M_D = -4.25$ ($r = 0.96 R_\odot$) in 1996. Since the density near $M_D = -4.25$, is of order 4×10^{-3}, and the downward velocity for the plumes is of order 5×10^4 cm s^{-1}, the estimated dynamical pressure of the plumes, ρv^2, is equal to or larger then 10^7 dyne cm^{-2}. The size of ρv^2 is comparable with the magnetic pressure, $B^2/8\pi$, corresponding to a field strength of $20 - 30$ kG. This demonstrates that a stable magnetized layer in the convection zone proper, may form when the complexity of convection motion is taken into account. If we wish to reproduce the observed temperature and irradiance variations by the magnetic field at the depth indicated by helioseismology, we find that B_m ranges from 20 kG to 47 kG during a solar cycle (choosing $B_0 = 90$ G). Therefore, in Figures 5-8 we also show this case (dotted curves: $M_{\rm Dc} = -4.25, \sigma = 0.5$). The irradiance fit ($\chi^2 = 1$) is also better than the effective temperature fit ($\chi^2 = 43$), the W parameter is equal to about 2×10^{-2}, and the predicted cyclic variation of solar radius is equal to about 2×10^{-5}, which can be tested by measuring the W parameter.

In fact, using MDI/SOHO data obtained between April 19, 1996 and June 24, 1998, Emilio et al (2000) found $W \leq 2 \times 10^{-2}$, which is consistent with the above prediction. This shows that the second case is in agreement with all relevant precise observations, including solar irradiance, effective temperature, radius, and p-mode oscillation observations. The first case is ruled out by the W parameter inferred from the observation.

4.2.3. *The upper part*

The upper part of the convection zone, $M_{\rm Dc} < -7.8$, is ruled out because the resulting irradiance and effective temperature variations are in antiphase with the solar cycle, which is in conflict with the observations.

In all cases, to produce the observed luminosity and effective temperature variations, the required magnetic field must increase with depth. The resulting W parameter also increases with depth. This is in agreement with the early studies (Däppen 1983; Endal et al 1985).

4.3. *The extended layer*

Another possibility is that these magnetic flux tubes are carried downwards into the stable subadiabatically stratified overshoot layer, to provide a seed field for the dynamo operating at the base of the convection zone. Therefore, the magnetic field extends from the convection zone to the overshoot layer. The following magnetic field distribution mimics this case,

$$F = \begin{cases} h(700) & M_D \geq M_{\rm Dc} \\ h(1) - 0.325(M_D - M_{\rm Dc}) & M_D \leq M_{\rm Dc} \\ h(1) + 1.3\exp[-2(M_D + 5.55)^2] & M_D \leq -5.55 \end{cases} \quad (19)$$

where $h(m) = (M_D/M_{\rm Dc})^m \exp[-m(M_D/M_{\rm Dc} - 1)]$. Choosing $M_{\rm Dc} = -1.55$ in equation (19) and $B_0 = 250$ G in equation (11), we also get a good fit to Figures 1 ($\chi^2 = 1$) and 2 ($\chi^2 = 40$). The magnetic field profile is depicted as a dashed curve in Figure 5. This case is also represented by dashed curves in Figures 6-8. The predicted W parameter is about 2×10^{-2}. It should be noted that what contributes to the observed cyclic variations of solar irradiance and effective temperature in this case, is

the field located within the convection zone proper, while the contribution of the field confined in the overshoot layer is negligible. MDI/SOHO data do not rule out this possibility.

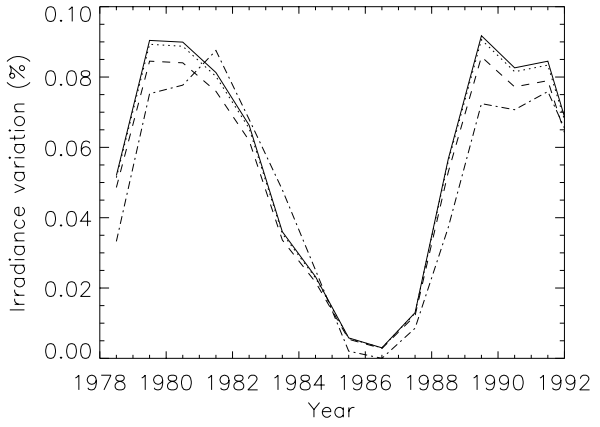

FIG. 6.— Comparison between the measured (dot-dashed curve) and calculated solar irradiance variations. The line style for the calculated is the same as that in Fig. 5.

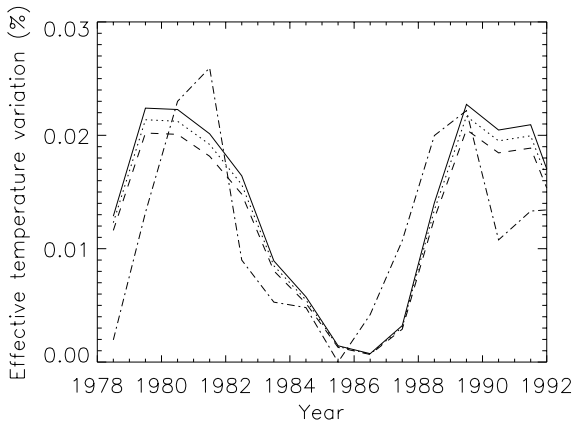

FIG. 7.— Comparison between the measured (dot-dashed curve) and calculated solar photospheric temperature variations. The line style for the calculated is the same as that in Fig. 5.

5. CONCLUSIONS

It is possible to locate solar interior magnetic fields using the observed cyclic variations of three global solar parameters such as luminosity, temperature and radius at the surface of the sun. This provides an alternative to helioseismology as a probe of the solar interior magnetic fields. Simultaneous measurements of solar total irradiance and effective temperature, can only select an allowed range of solar internal magnetic fields, which in terms of magnitude and location are consistent with helioseismic observations and recent MDI experiment on SOHO.

Although the observed cyclic variations of solar irradiance, effective temperature, radius and p-mode oscillation frequencies, require a magnetic field component between 20 and 47 kG, peaked at $r = 0.96R_\odot$ (within the convection zone proper), a stronger component of about 300 kG buried in the overshoot layer beneath the base of the convection zone cannot be ruled out, since the contribution of the latter to those observations is negligible.

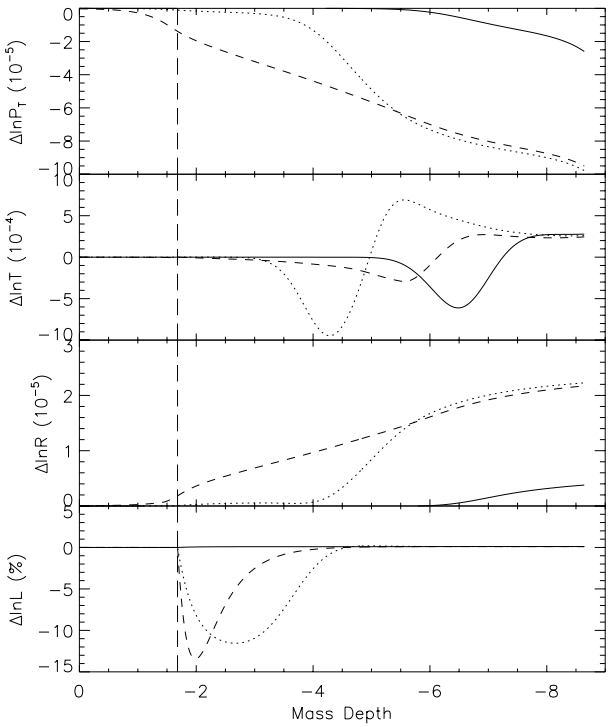

FIG. 8.— The structural changes caused by the magnetic field distributions given in Figure 5: relative pressure, temperature, radius and luminosity changes from top to bottom. The vertical line indicates the base of the convection zone. The line style for the calculated is the same as that in Fig. 5.

This work was supported in part by a grant from the National Aeronautics and Space Administration, and in part by Natural Science Foundation of China (project 19675064).

APPENDIX

AN ESTIMATE OF MAGNETIC EFFECTS ON THE RADIATIVE OPACITY

A magnetic field affects the absorption processes associated with free electrons, such as electron scattering absorption $\kappa_{\rm sc}$ and free-free transition absorption $\kappa_{\rm ff}$. We can estimate this effect in terms of the mean free paths with and without a magnetic field, l_B and l_0

$$\kappa_{\rm e0}/\kappa_{\rm eB} \propto (l_B/l_0)^2 \approx 1 + \tfrac{1}{4}(\gamma - 1)\tau_e^2\Omega_e^2 \qquad \text{(A1)}$$

Here $1/\tau_e$ is the collision frequency between electrons, $\kappa_e = \kappa_{\rm sc} + \kappa_{\rm ff}$ is the absorption component that will be affected by magnetic field and Ω_e is the electron cyclotron frequency. Magnetic fields also affect the bound-bound absorption, but this effect cannot be estimated easily by means of the classic method. Nevertheless, the quantum effect must be much smaller than the classic one described above.

The influence of magnetic fields on the radiative opacity can only be treated approximately, since we only use opacity tables. We assume that we can decompose the total opacity coefficient κ into two parts: $\kappa = \kappa_e + \kappa_1$, since $\kappa_{\rm sc}$ and $\kappa_{\rm ff}$ do not or only weakly depend on frequency (before taking the Rosseland mean). We use the opacity subroutine provided by YREC7 to calculate κ, and use equations (17.2) and (17.5) in Kippenhahn and Weigert (1990) to calculate κ_e. The opacity corrected by magnetic fields, κ', can be expressed approximately as follows

$$\kappa' = \kappa - \kappa_e \frac{(\gamma-1)\tau_e^2\Omega_e^2}{4+(\gamma-1)\tau_e^2\Omega_e^2}. \tag{A2}$$

The approximation originates from the fact that the absorption due to free-free transitions depends on frequency as $\kappa_\nu \propto \nu^{-3}$.

CONVECTION TEMPERATURE GRADIENT

When both χ and γ are considered to be variables, the convection temperature gradient $\nabla = (\partial \ln T/\partial P_T)_s$ (s stands for surroundings) can be expressed as follows

$$\nabla = \nabla_{\rm ad} + (y'/V'\gamma_0^2 C)(1+y'/V') - A_m, \tag{B1}$$

where the initial χ of the convection element is assumed to remain frozen in the surrounding material. $\nabla_{\rm ad} = (\partial \ln T/\partial \ln P_T)_S$ (S stands for entropy) is the adiabatic gradient and y' is obtained by solving the cubic algebraic equation,

$$0 = 2Ay'^3 + V'y'^2 + V'^2y' - V'. \tag{B2}$$

γ_0, C, V', A_m and A are defined by

$$\gamma_0 = [(c_{\rm p}\rho)/(2acT^3)][(1+(1/3)\omega^2/\omega], \tag{B3}$$

$$C = (g/l_m^2\delta)/8H_p, \tag{B4}$$

$$A_m = f'[(\nu/\alpha)\nabla_\chi + (\nu'/\alpha)\nabla_\lambda]\nabla_{\rm ad}, \tag{B5}$$

$$V' = 1/[\gamma_0 C^{1/2}(\nabla_{\rm rad} - \nabla_{\rm ad} + A_m)^{1/2}], \tag{B6}$$

$$A = (9/8)[\omega^2/(3+\omega_2)]. \tag{B7}$$

$\omega = \kappa\rho l_m$, g is the gravity acceleration, H_p is the pressure scale height, l_m is the mixing length and $\nabla_{\rm rad}$ is the radiative temperature gradient. f' is a dimensionless parameter that determines the influence of magnetic field on radiative loss of a convective element, $\nabla_\chi = (\partial \ln \chi/\partial \ln P_T)_s$, and $\nabla_\gamma = (\partial \ln \gamma/\partial \ln P_T)_s$. In general, magnetic fields tend to inhibit convection.

REFERENCES

Antia, H.M., Chitre, S.M., & Thompson, M.J. 2000, A&A, in press
Balmforth, N.J., Gough, D.O., & Merryfield, W.J. 1996, MNRAS, 278, 437
Brummell, N., Cattaneo, F. & Toomre, J. 1995, Science, 269, 1370
Caligar, P., Moreno-Insertis, F. & Schüssler, M. 1995, ApJ, 441, 886
Caligar, P., Moreno-Insertis, F. & Schüssler, M. 1998, ApJ, 502, 481
Däppen, W. 1983, A&A, 124, 11
Emilio, M., Kuhn, J.R., Bush, R.I. & Scherrer, P. 2000, ApJ, in press
Endal, A.S., Sofia, S. & Twigg, L.W. 1985, ApJ, 290, 748
Fröhlich, C. & Lean, J. 1998, in IAU Sympsium 185: New Eyes to See Inside the Sun and Stars, ed. F.L. Deubner, (Dortrecht: Kluwer Academic Publ.), 89
Gray, D.F. & Livingston, W.C. 1997a, ApJ, 474, 798
Gray, D.F. & Livingston, W.C. 1997b, ApJ, 474, 802
Guenther, D.B., Demarque, P., Kim, Y.-C., and Pinsonneault, M.H. 1992, ApJ, 387, 372
Kim, Y-C & Chan, K.L. 1998, ApJ, 496, L121
Kippenhahn, R. & Weigert, A. 1990, Stellar Structure and Evolution (Berlin: Springer-Verlag).
Lean, J.L., Cook, J., Marquette, W. & Johannesson, A. 1998, ApJ, 492, 390
Libbrecht, K.G. & Woodard, M.F. 1990, Nature, 345, 779
Lydon, T.J. & Sofia, S. 1995, ApJS, 101, 357
Lydon, T.J., Guenther, D.B. & Sofia, S. 1996, ApJ, 456, L127
Nordlund, Å 1999, IAU Colloquium 179 on Cyclical evolution of solar magnetic fields: Advances in theory and observations.
Prather, M.J. 1976, Ph.D. dissertation, Yale University.
Willson, R.C. & Hudson, H.S. 1991, Nature, 351, 42